INTERNATIONAL JOURNAL OF INTEGRATED ENGINEERING
ISSN: 2229-838X e-ISSN: 2600-7916

IJIE

Vol. 17 No. 9 (2025) 185-198
https://publisher.uthm.edu.my/ojs/index.php/ijie

Experimental and Numerical Study on the Impact of Air Gaps Between Layers on the Ballistic Performance of Steel-Rubber Laminated Composites

B. Bakri[1]*, M.S. Fadly[1], K. Anwar[1], S. Chandrabakty[1], Ricsen[1]

[1] *Mechanical Engineering Department of Universitas Tadulako*
Soekarno Hatta Street KM. 9, Palu, Central Sulawesi, 94148, INDONESIA

*Corresponding Author: bakri@untad.ac.id
DOI: https://doi.org/10.30880/ijie.2025.17.09.012

Article Info

Received: 19 December 2024
Accepted: 2 July 2025
Available online: 31 December 2025

Keywords

Composite, ballistic impact, steel, rubber, projectile

Abstract

Laminated steel–rubber composites are widely recognized for their capability to absorb and dissipate impact energy, making them promising candidates for ballistic protection. Despite their potential, the specific role of internal air gaps in influencing ballistic resistance has not been thoroughly explored. This research focuses on assessing how different air gap configurations affect the protective performance of these layered composites. A series of ballistic tests were carried out using 9 mm caliber hemispherical projectiles, supported by finite element simulations to replicate and validate the observed behaviors. Tests were conducted on specimens with varying air gaps between layers, including a configuration without any gap. The lowest penetration depth was observed in the specimen with no air gap, registering 6.502 mm in the experimental data and 6.885 mm in the simulation. Conversely, the highest penetration was recorded in the 3 mm air gap setup, reaching 10.357 mm and 10.092 mm for experimental and simulation results, respectively. Interestingly, the 2 mm air gap condition exhibited a notable rise in projectile kinetic energy, peaking at 547.6 J at 9.175×10^{-5} seconds, which then stabilized. These findings indicate that although greater air gaps allow deeper projectile intrusion, they effectively prevent back plate damage by concentrating stress absorption on the front layers. Overall, the study demonstrates that air gap design plays a critical role in controlling energy distribution and enhancing the impact resistance of steel–rubber composites.

1. Introduction

In recent years, numerous studies have focused on improving the effectiveness of bulletproof materials against projectile penetration, particularly for military applications. Ballistic resistance has been found to increase when a single plate is replaced by multiple thin plates arranged in layers. The sequence, number, and thickness of these layers significantly influence the material's failure characteristics under impact, resulting in varying levels of ballistic resistance across different designs. Additionally, considerable efforts have been made to enhance the performance of metallic structures subjected to high-velocity impacts [1-3]. One significant advancement is the application of rubber coatings on rigid materials to minimize damage caused by ballistic impacts and projectile penetration. Rubber's high capacity for absorbing energy makes it particularly effective at dissipating the kinetic energy of fast-moving projectiles. For this reason, it is commonly used as a protective layer in composite structures engineered to endure high-velocity impacts.

The issue of projectile impact on material targets has been studied for many years. Research has been conducted through experimental, numerical, and theoretical methods to examine the effects of ballistic impact on target materials. While there has been extensive investigation into the ballistic resistance of single plates, fewer studies have focused on layered targets that incorporate two or more materials. Amini et al. [4, 5] examined how single steel plates and steel-polyurea plates respond to ballistic impacts. The research, conducted both experimentally and numerically, concentrated on the failure modes and deformation of the plates. The findings revealed that adding a polyurea layer had a notable impact on the ballistic performance, especially when the layer was applied to the back of the steel plate. Wei et al. [6] explored the ballistic performance of layered metal plates with air gaps between each layer under impact from blunt projectiles. Their findings showed that plates with larger air gaps exhibited greater strength compared to those with smaller gaps. Additionally, the configuration of the layers influenced ballistic resistance, with a thicker first layer providing better protection than a thinner second layer.

Yunfei et al. [7] examined the ballistic performance of laminated steel plates made from various materials, impacted by projectiles with both ogival and blunt tips. The study revealed that the effect of target configuration on ballistic resistance decreases as the projectile's velocity increases. Additionally, the ballistic limit velocity for ogival projectiles was lower than that for blunt-nosed projectiles. Teng et al. [8-10] presented experimental and numerical studies on the ballistic resistance of laminated steel plates, showing that with blunt-tip projectiles, the ballistic limit velocity of laminated plates is 30% higher than that of single plates. Natural rubber, widely used as an impact damper in various engineering applications [11-14], offers excellent impact absorption, flexibility [15, 16], and tear resistance [17]. These properties make it ideal as a damping layer in composite structures. To enhance the ballistic resistance of laminated composites, air gaps are introduced between layers without increasing the material's overall thickness.

This study compares the ballistic performance of a single steel plate, a steel-rubber composite, and a steel-rubber composite with air gaps between layers. The goal is to identify the failure mechanisms of steel-rubber laminate composites subjected to 9 mm full metal jacket bullets. Numerical simulations complement experimental results by analyzing projectile velocity, energy absorption, and stress concentration in both the projectile and the target material.

2. Materials and Methods

The laminate composite consists of steel plates and rubber arranged in a 3-layer configuration, as illustrated in Figure 1. The composite panel has dimensions of 150x150 mm, with the steel plates being 3 mm thick and the rubber layer 4 mm thick. Based on previous references, air gaps of 1 mm, 2 mm, and 3 mm are inserted between the layers using spacers [6].

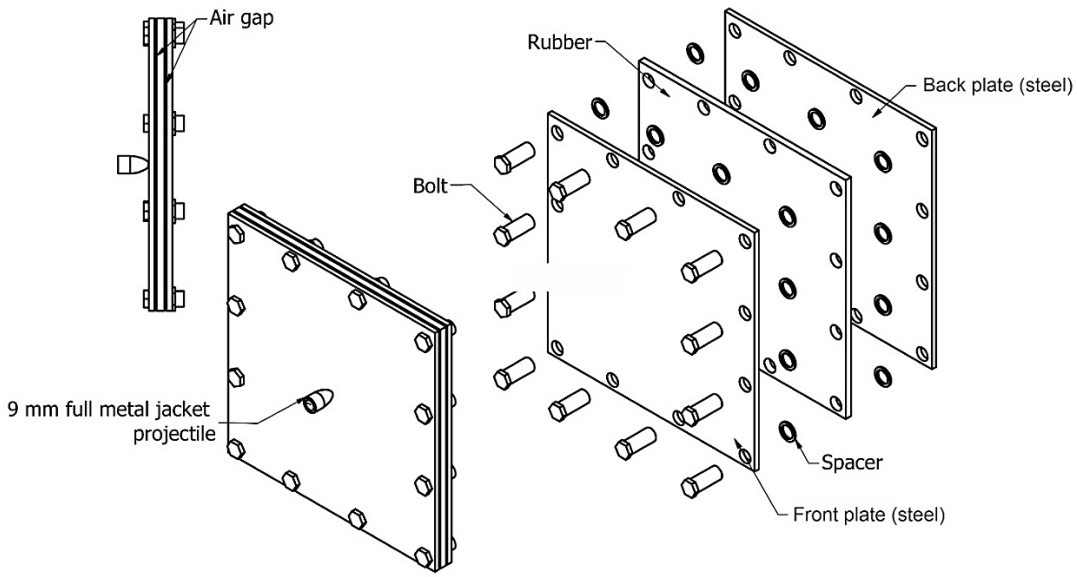

Fig. 1 *Manufacturing of steel - rubber composite laminate with air gaps*

The panel is assembled by bolting the front steel plate, rubber layer, and back plate together. Tensile tests are performed on the materials following ASTM D-638-03 for steel and ASTM D412 for rubber to assess their tensile strength, a key property in evaluating their ability to withstand forces. The stress-strain curves for both materials are shown in Figure 2. For the steel specimens, Type I samples were machined from steel sheets,

Int. Journal of Integrated Engineering Vol. 17 No. 9 (2025) p. 185-198

adhering to the standard dimensions, a gauge length of 50 mm, an overall length of 165 mm, and a narrow section width of 13 mm. Tests were conducted using a universal testing machine operated at a constant crosshead speed of 5 mm/min. For the rubber specimens, a Die C was used as specified in ASTM D412, featuring a gauge length of 33 mm and a reduced section width of 6 mm. Prior to testing, all rubber samples were molded and conditioned at room temperature for a minimum of 24 hours. The tensile tests for rubber were performed at a crosshead speed of 500 mm/min, following standard procedures to ensure consistency and reliability. These tensile tests provide essential data on the behavior of the steel-rubber composite under ballistic impacts and are also used to inform material models for numerical simulations.

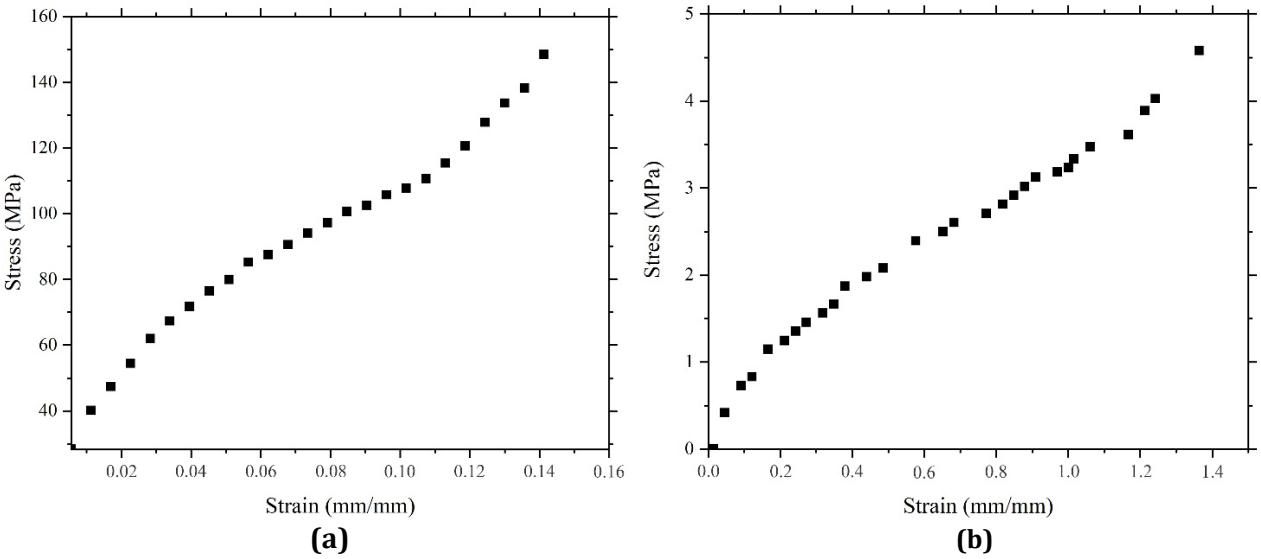

Fig. 2 *Comparison of stress-strain curves from the tensile tests: (a) steel; (b) rubber*

From Figure 2, the steel plate exhibits a maximum stress of 148.48 MPa with an elongation of 0.1413 mm/mm, while the rubber material shows a maximum stress of 4.58 MPa with an elongation of 1.3636 mm/mm. The average mechanical properties of steel and rubber materials are shown in Table 1.

Table 1 *Mechanical properties of steel and rubber*

Material	Max Stress (MPa)	ε (mm/mm)	Hardness	Impact Energy (J)	Tear Strenghth (N/mm)	Determination of compressions (%)
Steel	148.48	0.1413	118.21 BHN	63.48	-	-
Rubber	4.58	1.3636	67 Shore A	-	2.08	34.01

The ballistic testing conducted aligns with the research focus on the air gaps between the layers of the steel-rubber laminate composite. In the tests, a 9 mm full metal jacket bullet with a lead core and brass casing is fired from a distance of 5 meters at a 90° angle to the target. A pistol is used for firing, following the NIJ Standard 0101.06 for Ballistic Resistant Protective Materials. A chronograph sensor measures the projectile speed for each shot, and the testing scheme is depicted in Figure 3.

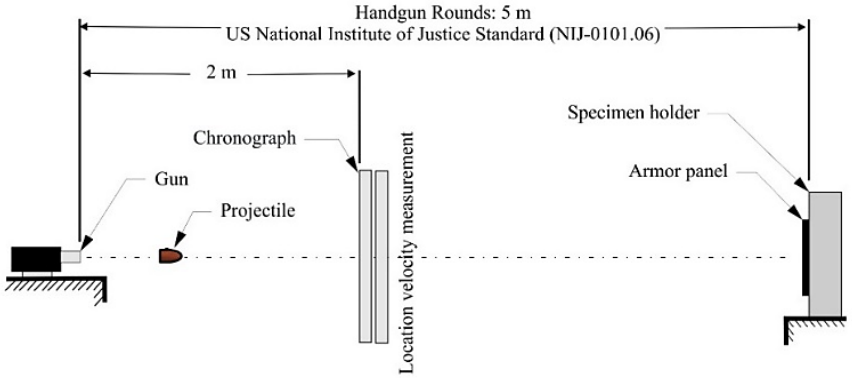

Fig. 3 *Schematic of the experimental setup*

The geometry of the projectile and composite panel in the numerical simulation is modeled to replicate the experimental setup. Before developing the finite element model, a mesh convergence study was carried out to verify that the simulation outcomes remained consistent regardless of mesh refinement. A total of nineteen mesh sizes, ranging from 0.2 mm to 2.0 mm, were tested. The simulated depth of penetration was then compared to experimental measurements, which yielded values of 6.885 mm and 6.502 mm, respectively. As illustrated in Figure 4, the convergence curve demonstrates that mesh sizes smaller than 0.8 mm produced stable results, indicating an acceptable level of accuracy for further analysis.

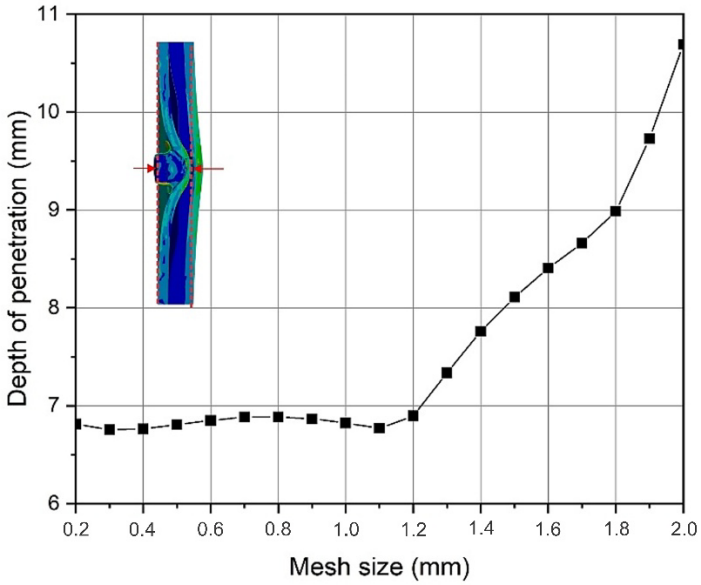

Fig. 4. *Mesh convergence curve of the depth of penetration*

The simulation, performed using Ansys Workbench 15.0 software with the finite element method, uses two meshing regions: fine meshing of 0.8 mm in the impact area and coarser meshing of 2 mm for areas away from the impact zone. Tetrahedral meshing is applied to both the projectile and the composite panel. The projectile itself has a uniform mesh size of 0.8 mm for both its core and outer layer. The meshing design is illustrated in Figure 5.

Int. Journal of Integrated Engineering Vol. 17 No. 9 (2025) p. 185-198

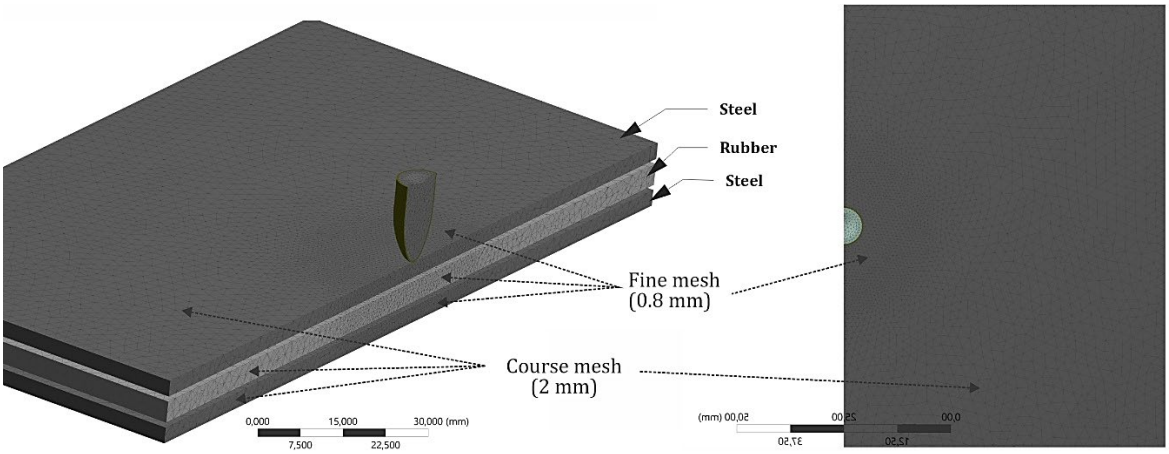

Fig. 5. *Meshing models in the numerical simulation*

The projectile load setting is determined by its initial velocity, measured using a chronograph sensor at a velocity of around 426 m/s. The boundary conditions apply fixed supports to each outer side of the composite panel's back plate. In the numerical simulations, both the projectile and the composite panel are modeled as flexible bodies to analyze the deformation during the ballistic impact. The contact between the bodies is modeled as frictionless. The load setting, specifically the bullet velocity of 426 m/s, along with the results of chronograph measurements and boundary conditions (fixed support), is illustrated in Figure 6.

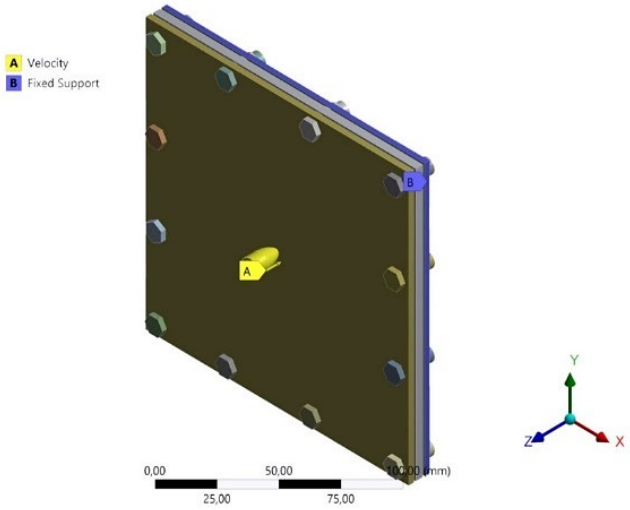

Fig. 6 *Load settings and boundary conditions*

In the numerical simulations, the Johnson-Cook material model [18-20] is applied to the steel plates and projectiles, as shown in Equation 1. For the rubber material, the Mooney-Rivlin material model [20-24] is used, as shown in Equation 2.

$$\sigma_{eq}=(A+B\,\varepsilon^{n})(1+C\ln\varepsilon^{\circ})\left(1-\left(\frac{T-T_o}{T_{melt}-T_o}\right)^{m}\right) \quad (1)$$

In this context, σ_{eq} represents the equivalent stress (Pa), A is the yield stress constant (Pa), B is the hardening constant, ε is the equivalent strain, n refers to the hardening exponent, C is the strain rate constant, m denotes the thermal softening exponent, ε° is the plastic strain rate, T is the test temperature (K), T_o is the room temperature (K), and Tmelt is the melting temperature (K).

$$\sigma_{eq}=2C_1\left[D-\frac{1}{D^3}\right]+2C_2\left[1-\frac{1}{D^3}\right] \quad (2)$$

In this case, σ_{eq} refers to the equivalent stress (Pa), C1 and C2 are probability constants (Pa), and D represents the extension ratio (Pa).

3. Results and Discussion

The target's capacity to absorb the kinetic energy of the projectile is measured by the depth of penetration, the deeper the projectile penetrates, the lower the ballistic strength. During both experimental and numerical simulations, the projectile causes the front plate to deform in the direction of its travel. Table 2 presents the penetration depth along with the corresponding energy absorption values for each tested configuration. Figure 7 shows the penetration depth for each configuration, while the ballistic impact results from both experimental and numerical simulations are presented in Figure 8.

Table 2 *Depth of penetration and energy absorbed for each configuration*

Configuration	Depth of penetration (mm)		Energy absorbed (J)	
	Average	Standard deviation	Average	Standard deviation
No air gap	6.502	0.44	478,86	5.28
Air gap 1 mm	6.945	0.32	476,10	7.51
Air gap 2 mm	8.909	0.56	547,60	4.78
Air gap 3 mm	10.357	0.51	509,79	4.21

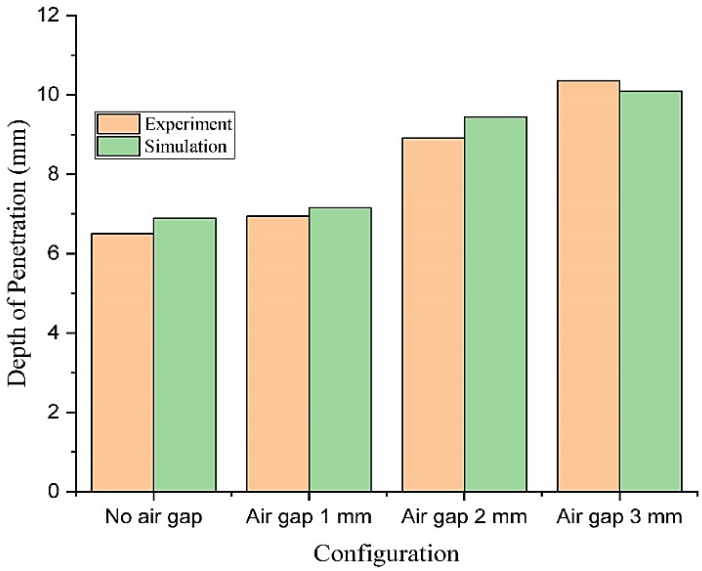

Fig. 7 *Target penetration depth at the end of ballistic impact*

As shown in Figure 7, the steel-rubber composite without an air gap has a shallower penetration depth compared to those with an air gap. Larger air gaps make it easier for the projectile to deform each layer, as there is less resistance to slow it down. Both the experimental results and numerical simulations show similar penetration depths, with an average error of 4.36%. The use of air gaps offers the benefit of reduced back plate protrusion. The larger the air gap, the less protrusion occurs, which improves safety for military applications. Figure 9 illustrates the projectile speed during penetration for each configuration, measured at 2.0×10^{-4} seconds.

Int. Journal of Integrated Engineering Vol. 17 No. 9 (2025) p. 185-198

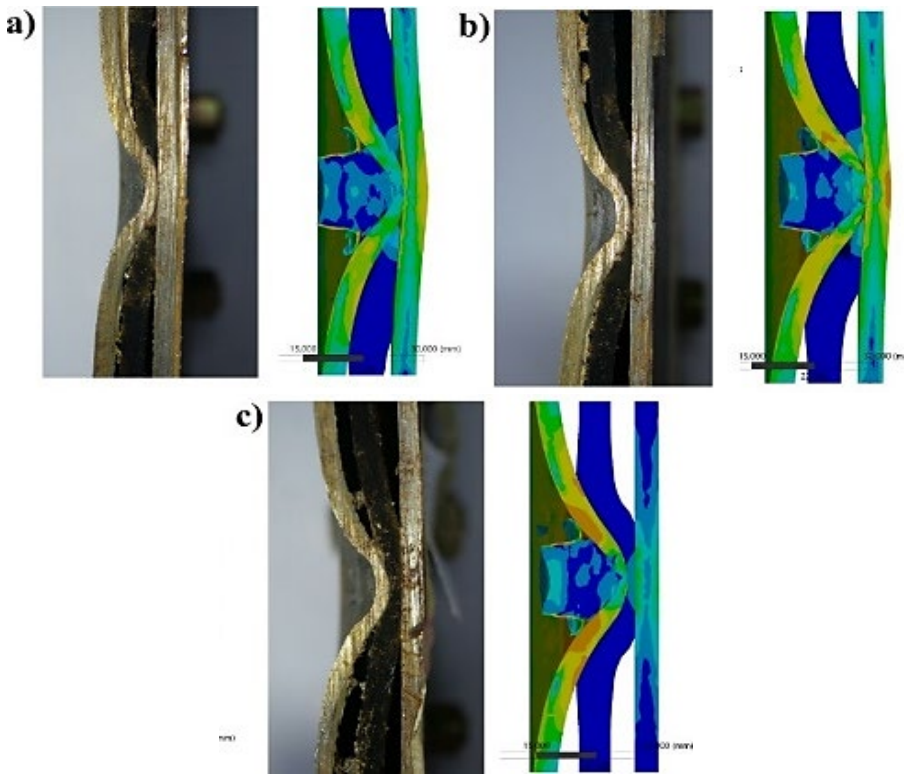

Fig. 8 *Ballistic impact for each configuration: (a) 1 mm air gap; (b) 2 mm air gap; (c) 3 mm air gap*

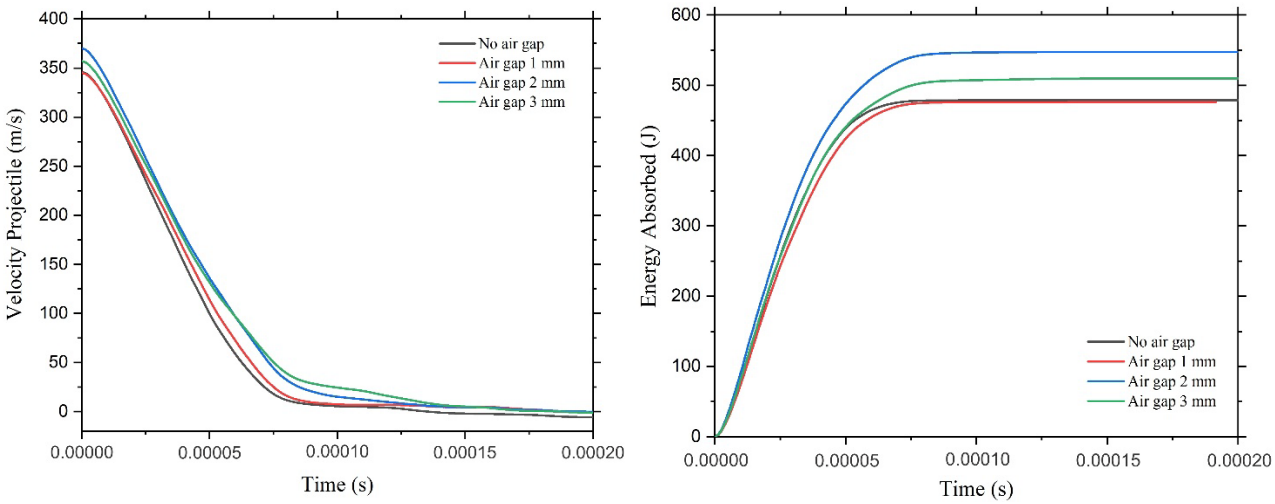

Fig. 9 *Projectile velocity & energy absorption during the penetration process*

Figure 9 shows that the projectile's velocity decreases over time as it penetrates the target, eventually reaching 0 m/s, or when the projectile can no longer penetrate. Steel-rubber composites without air gaps cause a quicker reduction in projectile velocity compared to those with air gaps, as the contact between layers adds resistance, hindering penetration. With larger air gaps, the decrease in velocity is slower, because the projectile takes longer to reach the rubber and back plate after penetrating the front plate. This leads to greater penetration depth in configurations with larger air gaps, as shown in Figure 7. The energy absorbed by each configuration increases immediately after the projectile penetrates the target, reaching a peak and then stabilizing. Figure 9 shows that a 2 mm air gap results in higher energy absorption compared to other configurations. With a 2 mm air gap, the energy rises significantly, reaching a maximum of 547.6 J at 9.175×10^{-5} seconds, and remains constant until the projectile stops penetrating the target. Each configuration absorbs different amounts of energy, as illustrated in Figure 10, which shows the total energy absorbed at the end of the ballistic impact. The amount of

energy absorbed was evaluated by measuring the reduction in the projectile's kinetic energy from the moment just before impact to the point after it had passed through the target.

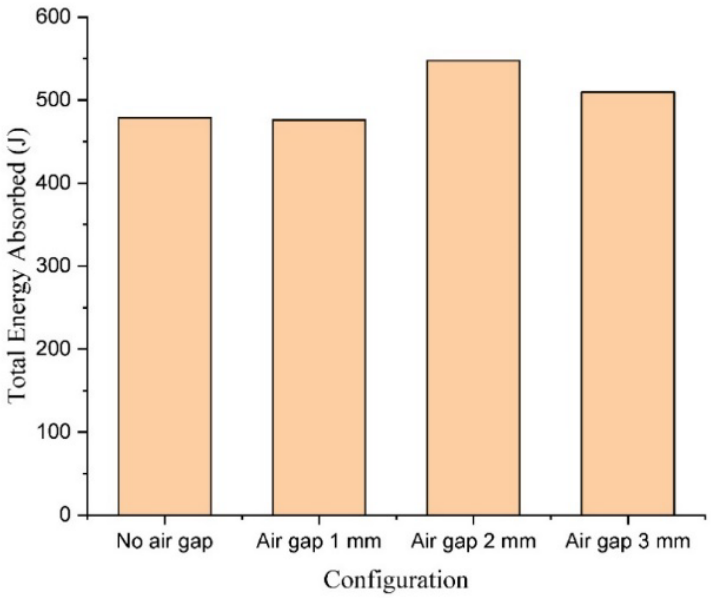

Fig. 10 *Total energy at the end of ballistic impact*

The configuration with a 1 mm air gap absorbs the least energy, at 476.1 J, followed by the configuration without an air gap at 478.8 J, and the 3 mm air gap configuration at 509.7 J. The highest energy absorption occurs with the 2 mm air gap configuration, reaching 547.6 J. This increase in energy absorption is linked to the kinetic energy retained by the target during the ballistic impact, with the projectile coming to a stop inside the target, indicating that all of its kinetic energy has been absorbed. Macro photos of each target configuration after impact are shown in Figure 11.

Int. Journal of Integrated Engineering Vol. 17 No. 9 (2025) p. 185-198

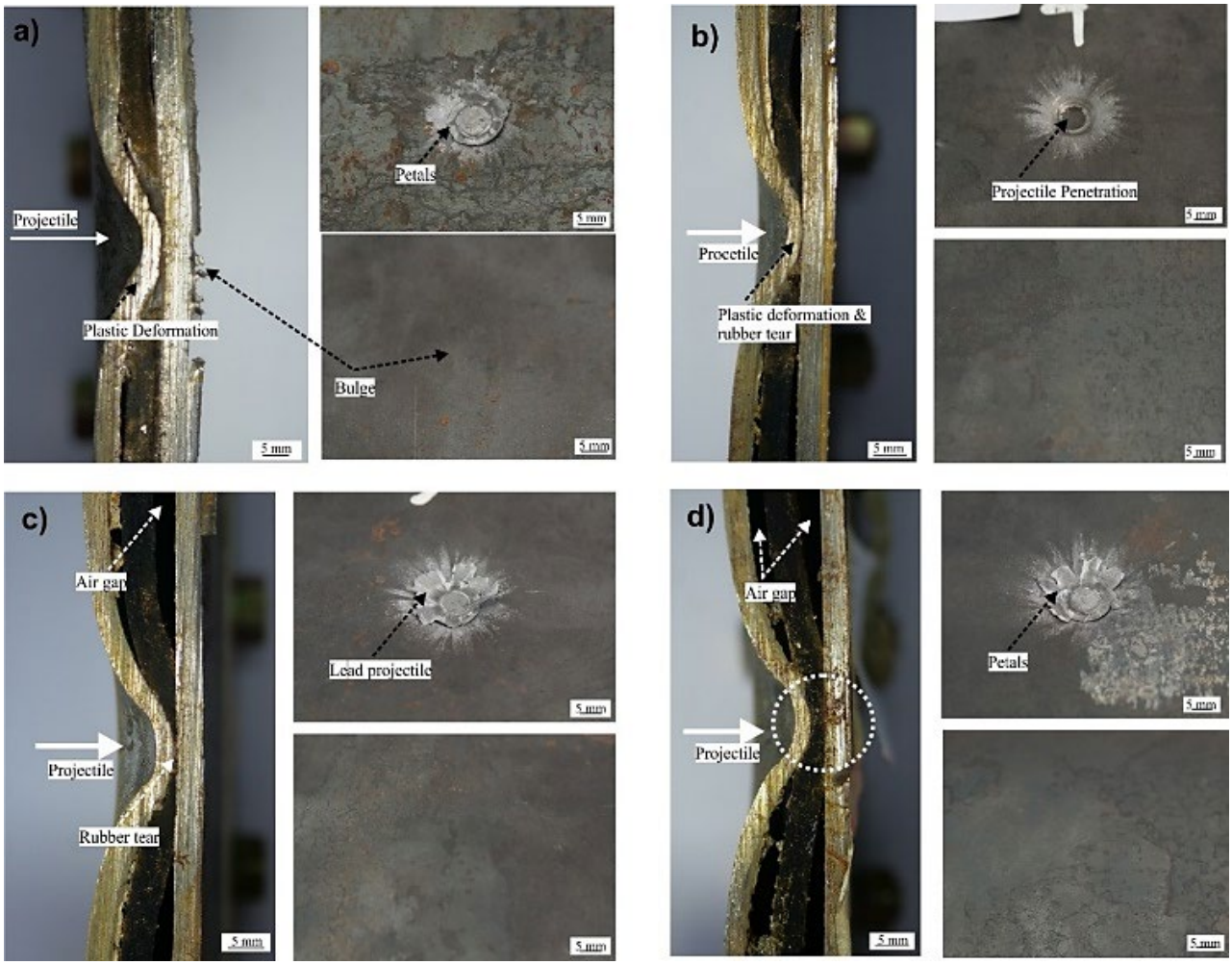

Fig. 11 *Macro photos of ballistic results: (a) without air gap; (b) 1 mm air gap; (c) 2 mm air gap; (d) 3 mm air gap*

Figure 11 presents the macroscopic characteristics of each target configuration from the cross-section, front, and back views. The deformation and perforation mechanisms are crucial for analyzing the ballistic impact on coated targets. In the configuration without an air gap (Figure 11a), the projectile fails to penetrate the target, but a tear is visible in the rubber layer. The high velocity of the projectile deforms the front plate, pushing the next layer and causing a bulge in the back plate. The front side shows petal-like deformations around the projectile. Configurations with air gaps show similar failure patterns, but the back plate remains free of bulges, and larger air gaps prevent the rubber layer from being penetrated. In all configurations, the projectile jacket adheres to the hole wall of the front plate, forming petals. The projectile leads to plastic deformation and tearing of the rubber layer. These results align with Ben-Door et al. [25], who concluded that high-speed impacts on ductile targets cause plastic deformation. Figures 12, 13, 14, and 15 show the numerical simulation results for ballistic impacts in each configuration.

The penetration of the projectile during the ballistic impact results in its residual velocity. The von Mises stress distribution is shown through color variations, with red indicating higher stress levels and blue showing lower stress. In the configuration without an air gap (Figure 12), the initial penetration occurs at 1.4451×10^{-5} seconds, reducing the projectile's velocity to 294.39 m/s. Deformation is concentrated on the front plate, causing the rubber layer to tear at 5.780×10^{-4} seconds. The projectile is stopped at 1.350×10^{-4} seconds, forming a bulge on the back plate. In configurations with air gaps, the decrease in projectile velocity slows as the air gap increases. The air gaps transfer stress indirectly to the next layer during initial penetration, reducing maximum stress in the rubber and back plates and minimizing damage. Larger air gaps also lead to deeper plastic deformation in the front plate, slowing the projectile further.

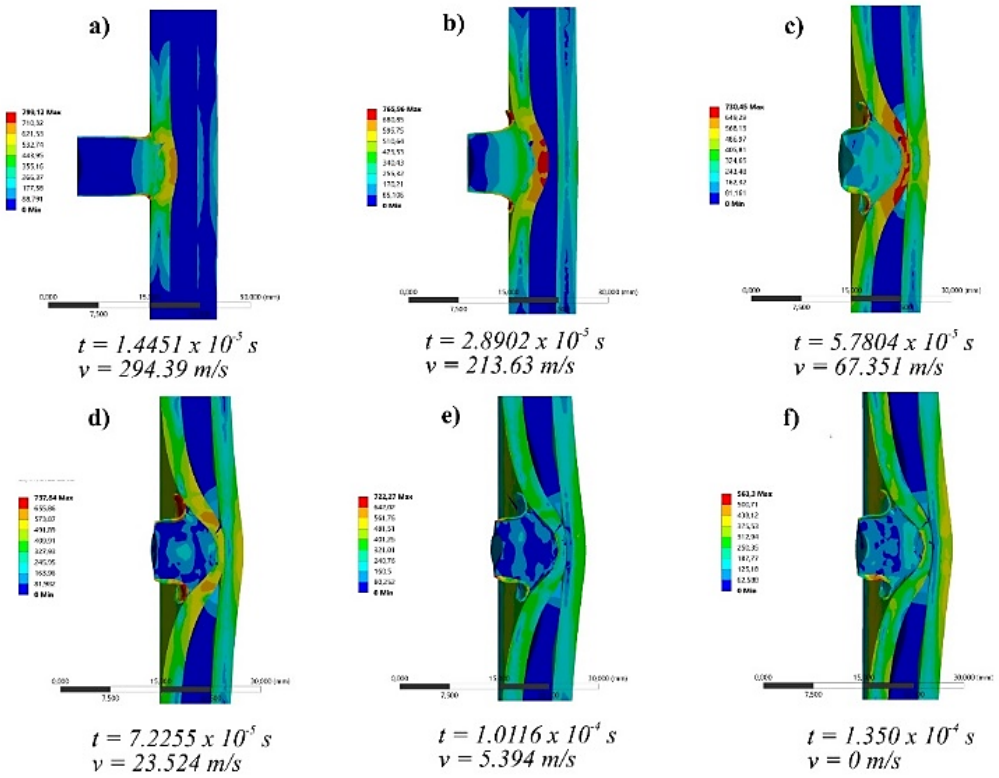

Fig. 12 *Von mises stress configuration for the case without an air gap*

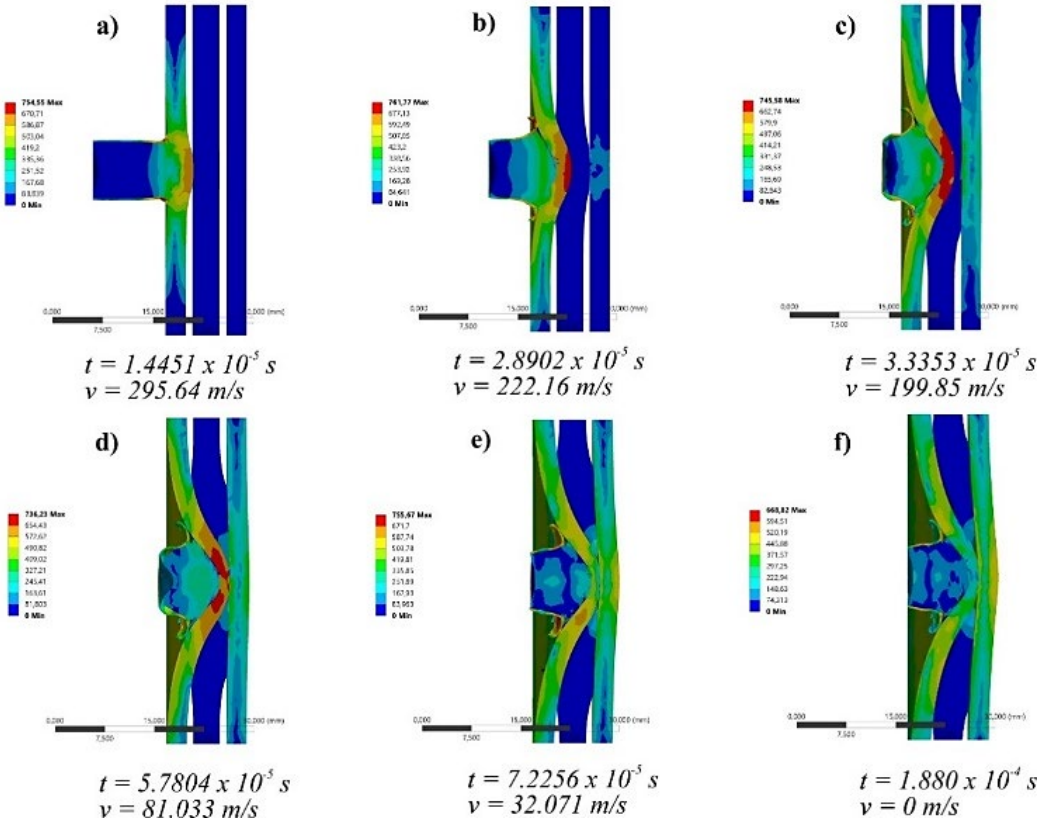

Fig. 13 *Von mises stress configuration for the case 1 mm air gap*

Int. Journal of Integrated Engineering Vol. 17 No. 9 (2025) p. 185-198

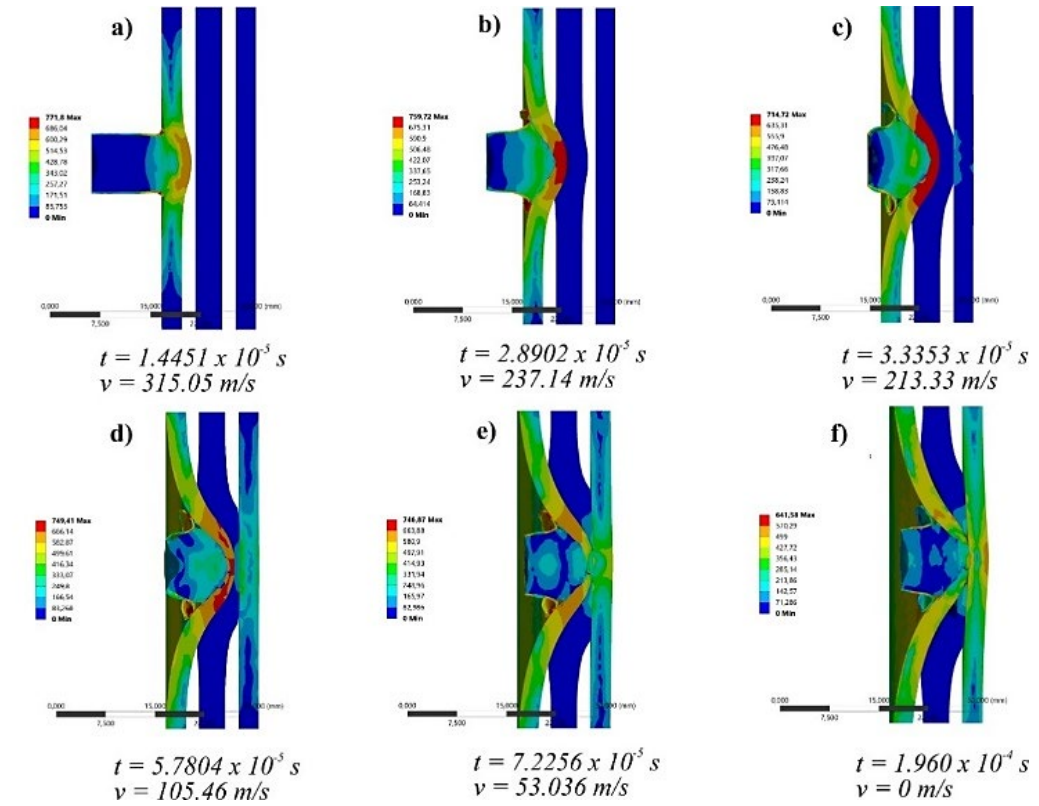

Fig. 14 *Von mises stress configuration for the case 2 mm air gap*

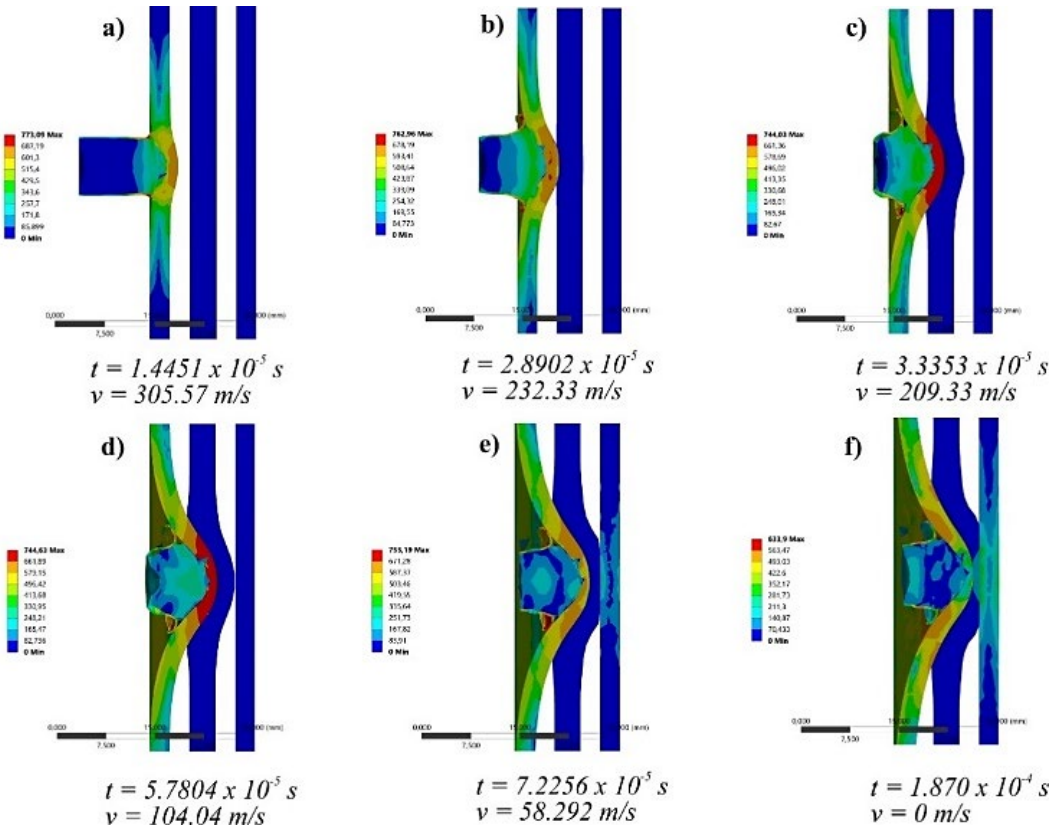

Fig. 15 *Von mises stress configuration for the case 3 mm air gap*

In the region near the penetration, substantial material deformation occurs due to the high pressure and friction from the projectile, altering the material's grain structure (Figure 16). Conversely, areas farther from the penetration path show a more stable microstructure with minimal deformation, as the projectile's kinetic energy does not reach those areas. This demonstrates that the projectile's energy is concentrated around the penetration site and diminishes with distance.

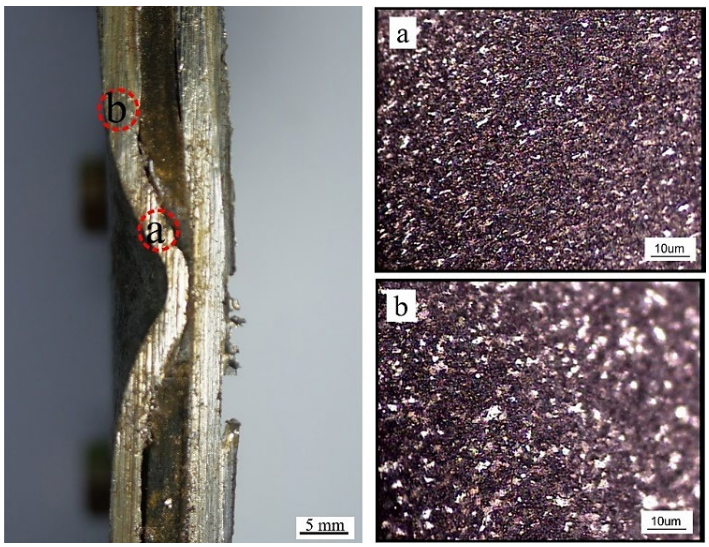

Fig. 16 *Micro-etching of the sample without an air gap after projectile impact: (a) near the projectile penetration channel; (b) away from the projectile penetration*

4. Conclusion

Steel-rubber composites with air gaps between layers help reduce back plate protrusion when impacted by a projectile. A smaller air gap leads to a faster reduction in projectile velocity, limiting the penetration depth on the front plate. In all configurations with air gaps, the projectile does not fully penetrate the target. A larger air gap also prevents damage or tearing of the rubber layer. Numerical simulations indicate that air gaps concentrate stress during the initial penetration of the front plate, preventing the immediate transfer of stress to subsequent layers. This suggests that in layered designs, the combination of hard front plates, rubber as a middle damping layer, steel back plates, and air gaps can effectively prevent the distribution of maximum stress to the following layers. This pattern suggests that the presence of an air gap does not provide an effective protective barrier. Instead, it gives the projectile more space to maintain its velocity and kinetic energy before striking the target. The gap delays direct contact, thereby reducing the initial resistance that a solid, continuous structure would typically provide.

Acknowledgement

The authors extend their gratitude to the Department of Mechanical Engineering, Universitas Tadulako, for offering analytical support during this research.

Conflict of Interest

Authors declare that there is no conflict of interest regarding the publication of the paper.

Author Contribution

The authors confirm their contributions to the paper as follows: ***study conception:*** *Bakri, Muhammad Syaiful Fadly, Ricsen;* ***data collection:*** *Bakri, Muhammad Syaiful Fadly, Ricsen;* ***analysis and interpretation of results:*** *Bakri, Muhammad Syaiful Fadly, Ricsen;* ***draft manuscript preparation:*** *Bakri, Muhammad Syaiful Fadly, Sri Chandrabakty, Khairil Anwar;* ***review and supervision:*** *Bakri. All authors reviewed the results and approved the final version of the manuscript.*

References

[1] Ackland, K., Anderson, C., and Ngo, T. D. (2013). Deformation of polyurea-coated steel plates under localised blast loading. International Journal of Impact Engineering, 51, 13–22. https://doi.org/10.1016/j.ijimpeng.2012.08.005

[2] Gamache, R. M., Giller, C. B., Montella, G., Fragiadakis, D., and Roland, C. M. (2016). Elastomer-metal laminate armor. Materials & Design, 111 , 362–368. https://doi.org/10.1016/j.matdes.2016.08.072

[3] Mohagheghian, I., McShane, G. J., and Stronge, W. J. (2017). Quasi-static and impact perforation of polymer-metal bi-layer plates by a blunt indenter. Thin-walled structures, 117, 35–48. https://doi.org/10.1016/j.tws.2017.03.036

[4] Amini, M. R., Simon, J., and Nemat-Nasser, S. (2010). Numerical modeling of effect of polyurea on response of steel plates to impulsive loads in direct pressure-pulse experiments. Mechanics of Materials, 42, 615–627. https://doi.org/10.1016/j.mechmat.2009.09.009

[5] Amini, M. R., Isaacs, J., and Nemat-Nasser, S. (2010). Investigation of effect of polyurea on response of steel plates to impulsive loads in direct pressure-pulse experiments. Mechanics of Materials, 42, 628–639. https://doi.org/10.1016/j.mechmat.2009.09.008

[6] Wei, Z., Yunfei, D., Sheng, C. Z., and Gang, W. (2012). Experimental investigation on the ballistic performance of monolithic and layered metal plates subjected to impact by blunt rigid projectiles. International Journal of Impact Engineering, 49, 115–129. https://doi.org/10.1016/j.ijimpeng.2012.06.001

[7] Yunfei, D., Wei, Z., Yonggang, Y., and Lizhong, S. (2014). Experimental investigation on the ballistic performance of double-layered plates subjected to impact by projectile of high strength. International Journal of Impact Engineering, 70, 38–49. https://doi.org/10.1016/j.ijimpeng.2014.03.003

[8] Teng, X., Wierzbicki, T., and Huang, M. (2008). Ballistic resistance of double-layered armor plates. International journal of impact engineering, 35, 870–884. https://doi.org/10.1016/j.ijimpeng.2008.01.008

[9] Teng, X., Dey, S., Børvik, T., and Wierzbicki, T. (2007). Protection performance of double-layered metal shields against projectile impact. Journal of mechanics of materials and structures, 2, 1309–1329. https://doi.org/10.2140/jomms.2007.2.1309

[10] Dey, S., Børvik, T., Teng, X., Wierzbicki, T., and Hopperstad, O. S. (2007). On the ballistic resistance of double-layered steel plates: an experimental and numerical investigation. International journal of solids and structures, 44, 6701–6723. https://doi.org/10.1016/j.ijsolstr.2007.03.005

[11] Yang, H., Yao, X.-F., Wang, S., Ke, Y.-C., Huang, S.-H., and Liu, Y.-H. (2018). Analysis and inversion of contact stress for the finite thickness Neo-Hookean layer. Journal of Applied Mechanics, 85, 101-108. https://doi.org/10.1115/1.4040598

[12] Khodadadi, A., Liaghat, G., Bahramian, A. R., Ahmadi, H., Anani, Y., Asemani, S., and Razmkhah, O. (2019). High velocity impact behavior of Kevlar/rubber and Kevlar/epoxy composites: a comparative study. Composite Structures, 216, 159–167. https://doi.org/10.1016/j.compstruct.2019.02.080

[13] Liu, F., Kong, X., Zheng, C., Xu, S., Wu, W., and Chen, P. (2018). The influence of rubber layer on the response of fluid-filled container due to high-velocity impact. Composite Structures, 183, 671–681. https://doi.org/10.1016/j.compstruct.2017.09.005

[14] Weerasinghe, D., Bambach, M. R., Mohotti, D., Wang, H., and Hazell, P. J. (2022). High-velocity projectile impact response of rubber-coated aramid Twaron fabrics. International Journal of Mechanical Sciences, 229, 107-115. https://doi.org/10.1016/j.ijmecsci.2022.107515

[15] Pouriayevali, H., Guo, Y. B., and Shim, V. P. W. (2011). A visco-hyperelastic constitutive description of elastomer behaviour at high strain rates. Procedia Engineering, 10, 2274–2279. https://doi.org/10.1016/j.proeng.2011.04.376

[16] Yang, H., Yao, X., Zheng, Z., Gong, L., Yuan, L., Yuan, Y., and Liu, Y. (2018). Highly sensitive and stretchable graphene-silicone rubber composites for strain sensing. Composites Science and Technology, 167, 371–378. https://doi.org/10.1016/j.compscitech.2018.08.022

[17] Hassim, N., Ahmad, M. R., Ahmad, W. Y. W., Samsuri, A., and Yahya, M. H. M. (2012). Puncture resistance of natural rubber latex unidirectional coated fabrics. Journal of Industrial Textiles, 42, 118–131. https://doi.org/10.1177/1528083711429144

[18] Grytten, F., Børvik, T., Hopperstad, O. S., and Langseth, M. (2009). Low velocity perforation of AA5083-H116 aluminium plates. International Journal of Impact Engineering, 36, 597–610. https://doi.org/10.1016/j.ijimpeng.2008.09.002

[19] Clausen, A. H., Børvik, T., Hopperstad, O. S., and Benallal, A. (2004). Flow and fracture characteristics of aluminium alloy AA5083–H116 as function of strain rate, temperature and triaxiality. Materials Science and Engineering: A, 364, 260–272. https://doi.org/10.1016/j.msea.2003.08.027

[20] Johnson, G. R., and Cook, W. H. (1985). Fracture characteristics of three metals subjected to various strains, strain rates, temperatures and pressures. Engineering fracture mechanics, 21, 31–48. https://doi.org/10.1016/0013-7944(85)90052-9

[21] Naarayan, S. S., and Subhash, G. (2017). Wave propagation in ballistic gelatine. Journal of the mechanical behavior of biomedical materials, 68, 32–41. https://doi.org/10.1016/j.jmbbm.2017.01.030

[22] Ravikumar, N., Noble, C., Cramphorn, E., and Taylor, Z. A. (2015). A constitutive model for ballistic gelatin at surgical strain rates. Journal of the mechanical behavior of biomedical materials, 47, 87–94. https://doi.org/10.1016/j.jmbbm.2015.03.011

[23] Kim, B., Lee, S. B., Lee, J., Cho, S., Park, H., Yeom, S., and Park, S. H. (2012). A comparison among Neo-Hookean model, Mooney-Rivlin model, and Ogden model for chloroprene rubber. International Journal of Precision Engineering and Manufacturing, 13, 759–764. https://doi.org/10.1007/s12541-012-0099-y

[24] Du, X. Bin, Zhao, Y. Q., Lin, F., and Xiao, Z. (2017). Parameters determination of Mooney-Rivlin model for rubber material of mechanical elastic wheel. In Applied Mechanics and Materials, 872, 198–203. https://doi.org/10.4028/www.scientific.net/AMM.872.198

[25] Singh, D. K., Banerjee, A., and Datta, D. (2024). Ballistic resistance of ceramic and metal target plates impacted against different projectile's nose shape: A numerical investigation. Mechanics of Advanced Materials and Structures, 1–13. https://doi.org/10.1080/15376494.2024.2400586